ZnO powders as multi-facet single crystals

Francia Haque, Stéphane Chenot, Francesc Viñes, Francesc Illas, Slavica Stankic, Jacques Jupille

PCCP

PAPER

View Article Online
View Journal

ZnO powders as multi-facet single crystals†

Cite this: DOI: 10.1039/c7cp01635b

Francia Haque,[a] Stéphane Chenot,[a] Francesc Viñes,[b] Francesc Illas,[b] Slavica Stankic *[a] and Jacques Jupille[a]

Received 14th March 2017,
Accepted 20th March 2017

DOI: 10.1039/c7cp01635b

Oxides are most commonly found in divided forms with properties difficult to control since their crystallographic orientations usually escape analysis. To overcome this an appropriate model system can be provided by ZnO smoke which, obtained by combustion of Zn in air, exhibits nanoparticles with well-defined surface facets. The present work focuses on the interaction of water with ZnO smokes by combining density functional theory based simulations and infrared spectroscopy measurements with applied pressures from 10^{-7} to 1 mbar. We demonstrate that the use of ultra-high vacuum allows the analysis of the very first stages of the adsorption, and report on water structures on ZnO($11\bar{2}0$) for the first time. We further show that ZnO powders behave as multi-facet single crystals involving ($10\bar{1}0$), ($11\bar{2}0$), (0001), and ($000\bar{1}$) surfaces with the polar orientations corresponding to 25% of the total surface area. A great deal of cross-agreements between experimental results and simulation provides a simple approach for the examination of hydroxylated/hydrated ZnO smokes and can be widely applied on other ZnO-related powders.

Introduction

The ubiquity of oxides in dispersed form has prompted research strategies in two directions: understanding the existing materials by means of appropriate reference systems and tailoring the desired properties through innovative syntheses.[1–4] Approaches based on the comparison of powders exhibiting oriented facets with their single crystal forms have been stimulated to pinpoint the orientation-dependent properties.[5–7] Alkaline earth oxides, MgO,[8–11] CaO,[9,12] SrO,[9] and BaO,[9] have long been studied in this context. The rock-salt structure leads to particles in the form of nanocubes closed by facets that show a unique (100) family of orientations that can be directly compared to single crystal surfaces.[5,8–13] They offer a test bed for the study of water[10,11,14–16] and hydrogen[17,18] reactivity on sites of defined coordination[9–11,17] as well as on specific defects that result from the contact between nanoparticles (NPs).[19] High density of coordinatively unsaturated sites combined with quantum confinement effects,[20] specific sites,[19] and electron trapping[21] at particle–particle interfaces triggers non-trivial behaviours in the ensembles of nanoparticles and make them specific objects that deserve direct examination. Examples are a significant enhancement of the photocatalytic efficiency of the P-25 titania powder when compared to any of its pure phases, rutile or anatase,[22] and the cooperative mechanism between charge carriers and surface orientations which drives photoreactivity.[23] The study of those synergistic effects requires a morphological control of photocatalysts through syntheses that reliably favours one orientation or the other.[23–25] A number of other oxides such as CeO_2, CuO, Co_3O_4, SnO_2, and Fe_2O_3 have been synthesized in the form of nanoparticles with well-defined facet orientations for the purpose of performing measurements of catalytic activity under controlled conditions.[4]

In this respect, zinc oxide nanoparticles appear as a quite challenging issue. ZnO is involved in numerous applications including paints, cements, ceramics, glasses, technical rubbers, sensors,[26,27] optical coatings,[28] solar cells[29] and catalysts.[30,31] It is, therefore, a massively produced material with global production of more than a million tons per year. The interest in this extremely useful material is boosted by the promising prospects in optoelectronics applications, although the difficulty of preparing p-type ZnO in a reproducible way is an obstacle for replacing GaN in devices.[32] The hunt for a better understanding of highly dispersed ZnO deals, however, with an extreme complexity stemming from the large spectrum of morphologies that ZnO powders exhibit – sticks, tetrapods, platelets, discs, rings, ribbons and spirals.[33,34] Despite the fact that both their growth and shaping are partly driven by the compensation required to stabilize polar orientations,[35,36] there is still a sense of discouragement over a seemingly intractable puzzle regarding such a fascinating collection of ZnO nanoforms.

A way out may be offered by the fact that divided ZnO powders mostly show four facet orientations, two non-polar,

[a] Sorbonne Universités, UPMC Univ Paris 06, CNRS-UMR 7588, Institut des NanoSciences de Paris, F-75252 Paris Cedex 05, France. E-mail: slavica.stankic@insp.jussieu.fr
[b] Departament de Ciència de Materials i Química Física & IQTCUB, Universitat de Barcelona, c/ Martí i Franquès 1-11, 08028 Barcelona, Spain

† Electronic supplementary information (ESI) available. See DOI: 10.1039/c7cp01635b

($10\bar{1}0$) and ($11\bar{2}0$), and two polar, ($000\bar{1}$) and (0001), the former being expected to dominate[37,38] in line with cleavage energies.[39] Water appears as an appropriate probe since comprehensive numerical simulations predict infrared spectra involving narrow infrared bands that are specific to each of the above orientations.[38] Given that powders are dominated by these orientations, water adsorption can act as a selective probe—as demonstrated by Kittaka and co-workers a long time ago.[39] In this work, infrared spectroscopy experiments are performed in the transmission mode on powders that are exposed to water from ultra-high vacuum conditions to near ambient pressure. In such a context, the application of ultra-high vacuum conditions is the key ingredient allowing a full control of the conditions upon adsorption. In a first row, it comprises the preparation of the required clean oxide surface and the observation of the very first stages of adsorption, and, in the second row, experimental data are then discussed in light of numerical simulations relying on a density functional approach aimed at the determination of energetically favourable water/ZnO surface configurations.

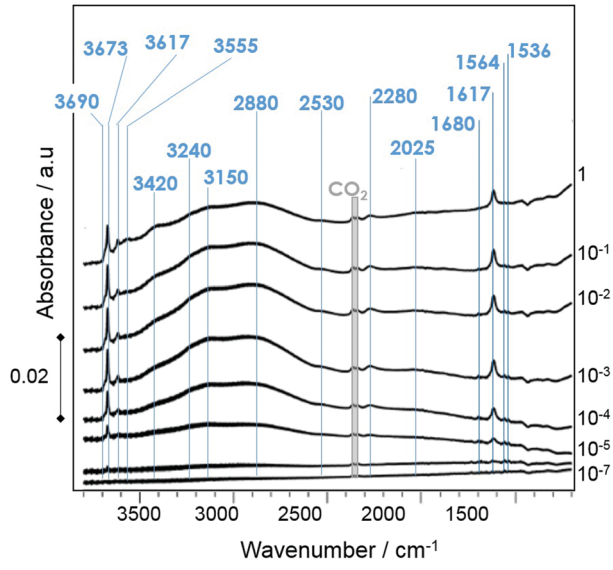

Fig. 2 Room-temperature FTIR spectra recorded in a vacuum (10^{-7} mbar) after exposure of ZnO smokes to P_{H_2O} = 10^{-7}–1 mbar, as indicated on the right hand side, mbar. The observed bands are indicated by vertical bars on which frequencies are given in cm^{-1}.

Results and discussion

Exposure of the ZnO smoke to water vapour

A representative SEM image of the ZnO smoke powder is shown in Fig. 1. These nanoparticles mostly adopt forms of sticks and tetrapods with sizes broadly varying. Stick and tetrapod morphologies are commonly observed in ZnO powders. In particular, tetrapods involve four prism-shaped wurtzite legs that extend in [0001] directions and present ($10\bar{1}0$) and ($11\bar{2}0$) facets on their sides. Surface energy calculations systematically show that sticks and tetrapods can be represented by Wulff construction that are dominated by ($10\bar{1}0$) and ($11\bar{2}0$) orientations with a minority of polar orientations[40] (see Fig. 1c, ref. 43 and references therein), in agreement with transmission electron microscopy.[40,44] ZnO smoke powders were exposed to increasing partial pressures of water vapour and the corresponding room-temperature Fourier transform infrared (FTIR) spectra recorded at P_{H_2O} = 1×10^{-7}–1 mbar are presented in Fig. 2. The observation of IR bands at very low pressures highlights the interest of performing experiments under ultra-high vacuum conditions. Frequencies shown in Fig. 2 are listed in Table S1 (see ESI†) where they are compared to measurements reported in ref. 6.

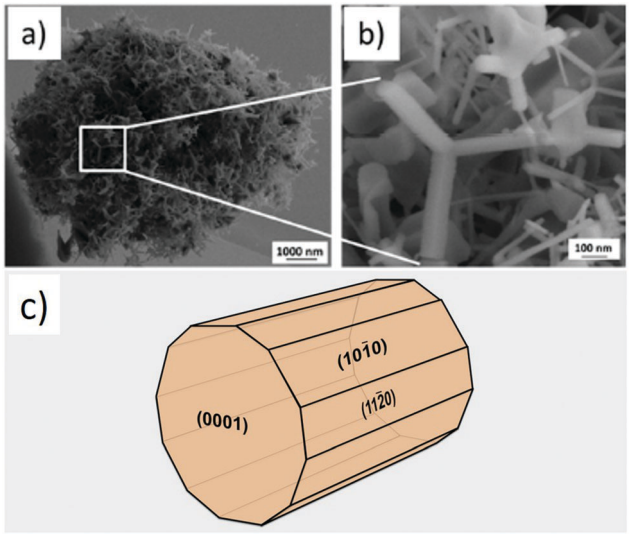

Fig. 1 Scanning electron microscope images of ZnO smoke: (a) an ensemble of nanoparticles and (b) a closer view of tetrapods and sticks present in the powder; (c) Wulff construction of ZnO stick derived from calculated surface energies[40] following Wulff shape construction,[41] as previously described.[42]

FTIR spectra recorded after exposure at a pressure of up to 1×10^{-1} mbar show a stable profile with bands progressively increasing in intensity. The spectra recorded after 300 s at 1×10^{-4} mbar (5000 L) and after exposures at 1 mbar show an astonishing similarity to the spectra recorded by Noei *et al.* after an exposure of 9000 L and after exposure to a partial pressure of 4 mbar of water vapour in helium,[6] respectively. The only difference is the absence of the sharp band at 3441–3448 cm^{-1} while the broad band at 3420 cm^{-1} is systematically observed. Such an agreement between the IR spectra recorded on ZnO smoke of the present work and the commercial ZnO powder[6] discards any fortuitous matching. Since water adsorption on ZnO leads to strongly orientation-dependent vibrational spectra,[38] the resemblance of the two IR spectra likely reflects a profound similarity of the orientation of the facets present on the two types of ZnO powders, which call for a detailed analysis.

Nevertheless, the adsorption of water on a given orientation may not lead to a unique configuration, as on ZnO($10\bar{1}0$) on which both fully dissociated and alternative half-dissociated arrangements of similar energy have been observed.[6,38,46–49] This has prompted us to compare the experimental data presented in Fig. 2 to theory, on the basis of a full theoretical review of the configurations that can be taken by water on the ($10\bar{1}0$), ($11\bar{2}0$),

(0001), and (000$\bar{1}$) facets, *i.e.* on the orientations expected to be dominant on ZnO nanoparticle surfaces.[37,38,45]

Comparison between experiment and simulation

ZnO(000$\bar{1}$)–O and ZnO(0001)–Zn polar orientations. Firstly, it has been found that the water adsorption gives rise to only one structure on each basal plane. Experiment and theory fully agree about water adsorption on the polar (000$\bar{1}$) orientation (Fig. 3). Hydroxyl groups are expected to stand up on this surface giving rise to a unique OH stretching band in the frequency region under study.[38] In the present work, it is found at 3617 cm^{-1}—matching well with the values recorded by HREELS on a ZnO(000$\bar{1}$) single crystal and by FTIR on ZnO powder, *i.e.* 3621 and 3620 cm^{-1}, respectively.[6] The hydroxylation of the zinc-terminated ZnO(0001)–Zn surface is not expected to be observed in the IR spectra since the intensity of the related O–H stretching band is predicted to be too weak.[38]

ZnO(10$\bar{1}$0) orientation. On the ZnO(10$\bar{1}$0) orientation, four calculated configurations have been selected (Fig. 4). Additional structures were found as well, but the present choice was limited to those configurations which can unambiguously explain at least one experimentally observed IR band.

Those correspondences are discussed first. The (2 × 1) structure (labelled $(2 \times 1)_A$), in which every second water molecule is dissociated,[38,47–49] is confirmed by the present DFT approach to be the most stable configuration for water adsorption on ZnO(10$\bar{1}$0) (Fig. 4b). The dissociation, which is partly triggered by hydrogen bonds between water molecules, gives rise to free O_w–H groups attached to surface zinc atoms Zn_s of a Zn–O dimer row and to a proton adsorbed on a surface oxygen atom O_s of a neighbouring dimer row. The resulting O_s–H groups are hydrogen-bonded across the [11$\bar{2}$0] trenches to the free O_w–H. DFT predicts stretching frequencies of 3763 and 3139 cm^{-1} for Zn_s–O_wH and O_s–H, respectively. The corresponding experimental modes are at 3673 and 3150 cm^{-1} (Fig. 4a), which

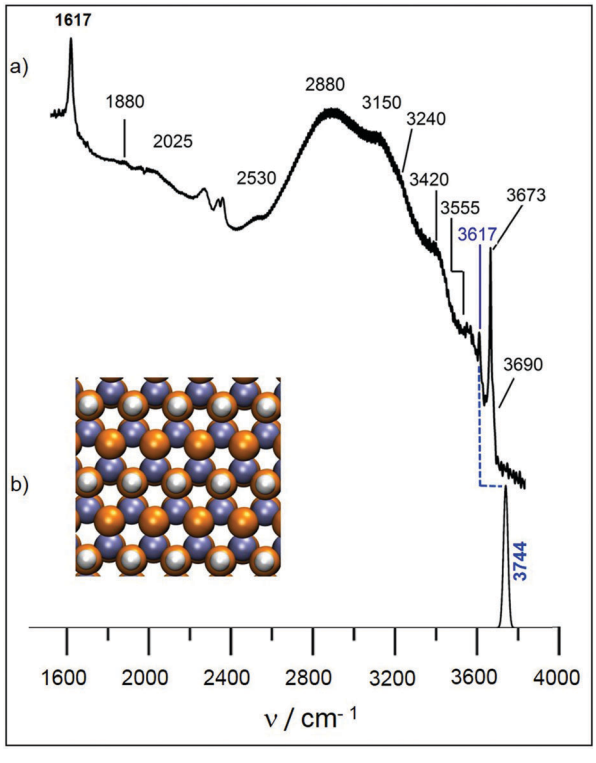

Fig. 3 Comparison between (a) IR spectrum recorded on ZnO smoke at RT after exposure to P_{H_2O} = 1 mbar—representative of the spectra shown in Fig. 2—and (b) calculated spectra associated with the H_2O adlayer structure determined by the DFT approach for the ZnO(000$\bar{1}$) surface which involves a unique ν_{OH} stretching frequency (see the text). On the left, schematic representation of the surface structure in which, substrate Zn, substrate O, and H atoms are represented by blue, orange, and grey, respectively.

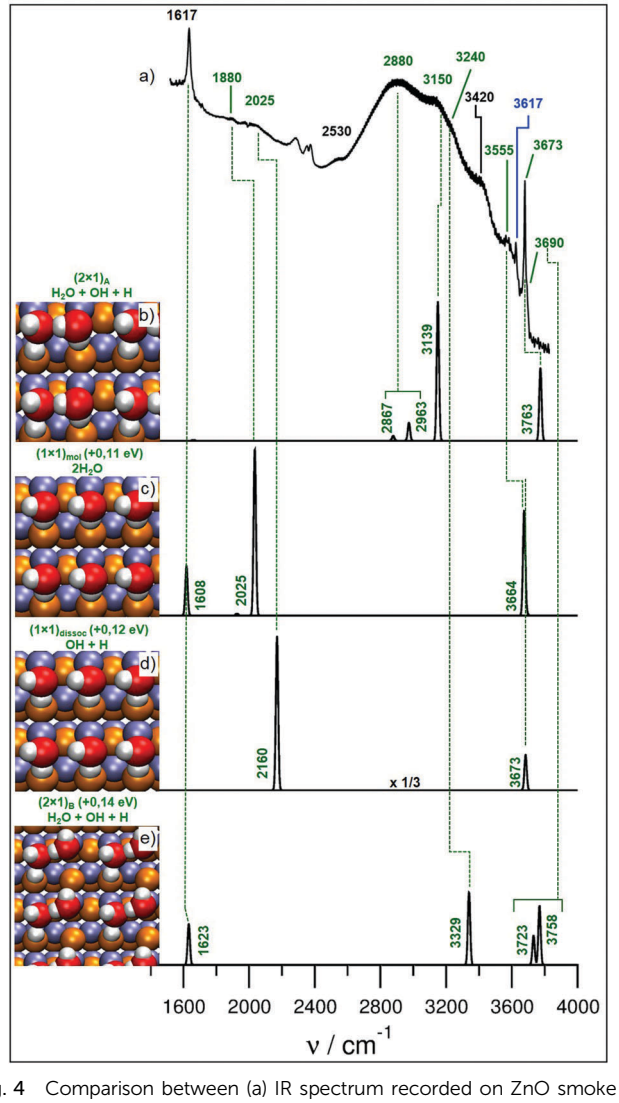

Fig. 4 Comparison between (a) IR spectrum recorded on ZnO smoke at RT after exposure to P_{H_2O} = 1 mbar—representative of the spectra shown in Fig. 2—and calculated spectra associated to H_2O adlayer structures determined by DFT approach for ZnO(10$\bar{1}$0) surface: (b) $(2 \times 1)_A$, (c) $(1 \times 1)_{mol}$, (d) $(1 \times 1)_{dissoc}$ and (e) $(2 \times 1)_B$. The four calculated structures are presented in the figure on the left hand side of these spectra. The extra energy involved in those structure with respect to the $(2 \times 1)_A$ structure are indicated. Oxygen and zinc atoms from the substrates appear as blue and orange spheres, respectively, whereas oxygen and hydrogen from the adsorbed water molecules are represented by red and light grey, respectively. Blue highlighted frequency corresponds to ZnO(000$\bar{1}$)–O orientation.

parallel values of 3670 and 3195 cm^{-1} recorded on the $(10\bar{1}0)$ surface of a ZnO single crystal (see the ESI†).[6,46] The comparison with the vibrational spectra recorded on single crystal surfaces makes the assignment quite reliable. The non-dissociated water molecules involved in the $(2 \times 1)_A$ structure are hydrogen-bonded to both neighbouring free OH and surface oxygen atoms of the next ZnO dimer rows, which is expected to give rise to DFT symmetric and asymmetric stretches at 2963 and 2867 cm^{-1}, respectively (Fig. 4b). The experimental counterpart is the broad band at 2880 cm^{-1} (Fig. 4a). This interpretation contradicts the assignment of the mode seen at 3690 cm^{-1} to a non H-bonded O_w–H of the intact water molecule.[46] The origin of this mode is discussed in connection with the additional configurations of water adsorbed on ZnO$(10\bar{1}0)$ (see below). Calculations reveal the existence of three additional H_2O/ZnO$(10\bar{1}0)$ superstructures that are energetically almost degenerate with the above $(2 \times 1)_A$. These involve fully molecular $(1 \times 1)_{mol}$ (Fig. 4c), fully dissociated $(1 \times 1)_{dissoc}$ (Fig. 4d), and alternative half-dissociated $(2 \times 1)_B$ structures (Fig. 4e). They are higher in energy than the $(2 \times 1)_A$ structure only by 0.11, 0.12 and 0.14 eV per molecule, respectively. The coexistence of the $(1 \times 1)_{mol}$ structure with the half-dissociated $(2 \times 1)_A$ has already been postulated on the basis of STM observations supported by DFT calculations.[47] In the $(1 \times 1)_{mol}$ structure, water molecules occupy similar sites to the non-dissociated water molecules of the $(2 \times 1)_A$ arrangement (Fig. 4c and ref. 47). The calculated bands at 1608 and 1623 cm^{-1} can be assigned to the deformation mode of water, whose main feature is observed experimentally at 1617 cm^{-1}. Discussion about this mode requires, however, a complete overview of all the configurations that are identified in the IR spectra of the hydroxylated ZnO smoke and is, therefore, given at the end of this section. The two bands of the calculated vibrational spectrum, at 3664 and 2025 cm^{-1}, correspond to the free O_w–H and the hydrogen-bonded O_w–H, respectively. The former is associated with the well-defined experimental feature observed at 3555 cm^{-1} (Fig. 4a) which, in the same way as in the calculated spectra, is shifted by about a hundred wave numbers with respect to the intense stretching Zn_s–O_wH band (3673 cm^{-1}) related to the $(2 \times 1)_A$ structure (Fig. 4a). The calculated 2025 cm^{-1} band is related to the experimental mode observed at 1880 cm^{-1} (Fig. 4a).

Direct observation by STM[47] of $(1 \times 1)_{mol}$ makes very likely the occurrence of both, the fully dissociated $(1 \times 1)_{dissoc}$ (Fig. 4d) and the alternative half-dissociated $(2 \times 1)_B$ (Fig. 4e) since being of similar energy to $(1 \times 1)_{mol}$. DFT predicts that the dissociation of the molecules of $(1 \times 1)_{mol}$ yields the $(1 \times 1)_{dissoc}$ structure which involves free O_w–H (3673 cm^{-1}) and hydrogen-bonded O_s–H (2160 cm^{-1}) groups (Fig. 4d). The DFT value of 2160 cm^{-1} is related to the experimental 2025 cm^{-1} (Fig. 3a). (Because of the systematic blue shift of the calculated frequencies, it is consistent to assign the calculated 2025 cm^{-1} ($(1 \times 1)_{mol}$, Fig. 4c) and 2160 cm^{-1} ($(1 \times 1)_{dissoc}$, Fig. 4d) to the experimental bands at 1880 cm^{-1} and 2025 cm^{-1}, respectively.) Moreover, the two calculated bands are the only counterparts that can be found in the whole set of calculated spectra for the modes that are observed in the 1850–2025 cm^{-1} range. Finally, in the additional half-dissociated $(2 \times 1)_B$ (Fig. 4e), adsorbed moieties occupy similar sites to those in $(2 \times 1)_A$, except that each water molecule draws a free O_w–H outward instead of being doubly hydrogen-bonded (Fig. 3a), which results in two O_w–H stretches with DFT values of 3723 and 3758 cm^{-1}. Together with the free O_w–H mode of the $(1 \times 1)_{dissoc}$ structure (a DFT value of 3673 cm^{-1}), these modes can be related to the IR features experimentally observed at 3690–3700 cm^{-1} (this work and ref. 44) and 3656 cm^{-1},[46] in the vicinity of the sharp Zn_s–O_wH band (3673 cm^{-1} in the experimental spectra) that dominates the $(2 \times 1)_A$ configuration. The occurrence of these features in the HREELS spectrum of the ZnO$(10\bar{1}0)$ crystal surface[6] definitely demonstrates that they are related to hydroxylated ZnO$(10\bar{1}0)$. Although precise assignments cannot be provided, the experimental observation of additional bands at 3639, 3656, and 3690 cm^{-1} (Fig. 4a and ref. 6) around the intense Zn_s–O_wH mode at 3673 cm^{-1} ($(2 \times 1)_A$ configuration, Fig. 4b) supports the existence of the $(1 \times 1)_{dissoc}$ (Fig. 4d) and $(2 \times 1)_B$ (Fig. 4e) configurations that provide calculated counterparts to the observed frequencies. Finally, H-bonded O_s–H of $(2 \times 1)_B$ (Fig. 4e) is blue-shifted (DFT: 3329 cm^{-1}) with respect to that of $(2 \times 1)_A$ (DFT 3139 cm^{-1}) and it is attributed to the broad although well-defined mode experimentally observed at 3240 cm^{-1} (Fig. 4a).

ZnO$(11\bar{2}0)$ orientation. In contrast to the ZnO$(10\bar{1}0)$ surface, there exist no experimental data for water adsorption on the ZnO$(11\bar{2}0)$ single crystal surface. To our knowledge, the interaction between water and the ZnO$(11\bar{2}0)$ surface has been discussed only through theoretical approaches.[38,49–51] By comparison with experiment (Fig. 5a), the present DFT calculations

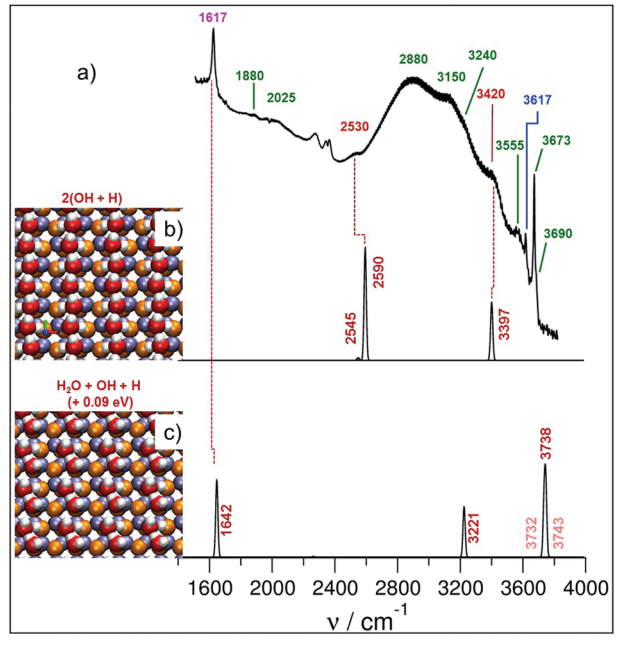

Fig. 5 Comparison between (a) IR spectrum recorded on ZnO smoke at RT after exposure to P_{H_2O} = 1 mbar—representative of the spectra shown in Fig. 2—and the calculated spectra associated with H_2O adlayer structures determined by the DFT approach for the ZnO$(11\bar{2}0)$ surface and representative structures: (b) $(2 \times 1)_{fully\text{-}disocc}$, (c) $(2 \times 1)_{half\text{-}dissoc}$. The same colour code as in Fig. 3 and 4 is used for spheres representative of atoms. The blue and green highlighted frequencies correspond to ZnO$(000\bar{1})$–O and ZnO$(10\bar{1}0)$ orientations, respectively. The deformation frequency (1617 cm^{-1}) of the water molecule is highlighted in violet.

favour the full dissociative adsorption of water molecules (Fig. 5b) by 0.09 eV with respect to a half-dissociation (Fig. 5c) similar to that observed on ZnO($10\bar{1}0$)—that is in agreement with the calculations of other groups.[49,50] Although the view is not unanimous,[51] all groups agree that the configuration of lowest energy is any of the two above structures and that their energy separation is $\sim$0.1 eV per molecule or less. The fully molecular adsorption is discarded since its difference in energy with the structure of lowest energy lies between 0.25 eV per water molecule (this work) and 0.85 eV per water molecule in ref. 43. As in the case of water-covered ZnO($10\bar{1}0$), the small difference in energy between fully dissociated and half-dissociated configurations points to coexisting superstructures. The fully dissociated (2×1) involves only hydrogen bonded OH groups (Fig. 5b) predicted to give rise to modes at 3397 and 2590 cm^{-1} as well as a fairly weak mode at 2545 cm^{-1}. These are associated with experimentally recorded bands at 3420 and 2530 cm^{-1}, respectively (Fig. 5a). The assignment is meaningful since the two bands could not be explained by any other water structure among those that are presented herein, which is a necessary condition to support the reliability of the configuration proposed for adsorption of water on ZnO($11\bar{2}0$). In the second structure suggested herein, the half-dissociated (2×1) (Fig. 5c) vibrational modes are expected at 3738, 3221, and 1642 cm^{-1}. None of these can be singled out on the basis of the experimental IR spectra, although they do not contradict the experimentally observed data (Fig. 5a). Despite the fact that this structure has no unambiguous counterpart in the experimental infrared spectrum, its existence is assumed because of its very small difference in energy with the fully dissociated (2×1).

According to calculations, the deformation mode of water molecules, exhibiting a rather high intensity, does not appear in any of the most stable water configurations—the $(2 \times 1)_A$ structure for ZnO($10\bar{1}0$) (Fig. 4b) and the fully dissociated (2×1) for ZnO($11\bar{2}0$) (Fig. 5b). Four bands are identified in the experimental spectrum, at 1536, 1564, 1617, and 1680 cm^{-1} (Fig. 2). A consistent DFT counterpart is offered by the three modes found in the calculated configurations, at 1608 cm^{-1} ($(1 \times 1)_{mol}$, Fig. 4c), 1623 cm^{-1} ($(2 \times 1)_B$, Fig. 4e) and 1642 cm^{-1} (half-dissociated (2×1), Fig. 5c), although unambiguous assignments are not possible. Finally, by comparing the calculated intensities (Fig. 4 and 5 and ref. 38) to the experiment, a non-polar/polar ratio of 75/25 is determined. It is close to other estimates[37,38] and consistent with the general expectation that the non-polar ($10\bar{1}0$) and ($11\bar{2}0$) are dominant orientations on the ZnO surface exhibiting lowest cleavage energy.[45]

Experimental and computational methods

Experimental

The present work deals with ZnO nanopowders obtained by burning zinc in an air atmosphere. This method allows for the formation of oxide particles at temperatures high enough to be close to the equilibrium shape.[11] Similar to MgO smokes,[52] also the obtained ZnO smoke powders include nanoparticles of a broadly dispersed size while being mostly in the form of sticks and tetrapods that are commonly encountered in ZnO powders (Fig. 1). ZnO smokes are deposited on $\sim 25 \times 25$ mm^2 silicon wafers that are set above the burning zinc ribbon. Silicon supports allow *in situ* FTIR analysis by transmission since silicon is transparent in the frequency range of relevance.[53] ZnO smokes show a rather low specific area of 4 m^2 g^{-1}, as determined by nitrogen sorption measurements. This modest specific area has a remarkable advantage regarding reactivity measurements. Typically, ZnO deposited on the $\sim 25 \times 25$ mm^2 Si wafer amounts to $\sim$1 mg, which corresponds to an area of 40 cm^2. On the basis of the kinetic theory of gases, this means that $\sim$10 s are required at a partial pressure of 1×10^{-6} mbar for an exposure of the surface of the oxide as a whole to 1 Langmuir (symbol L, exposure of 1.33×10^{-6} mbar during 1 second which corresponds to a full monolayer if the sticking probability is assumed to be one). Exposures being systematically of 300 s ensure that, even at the smallest pressure used herein (1×10^{-7} mbar), all the surface sites of the powder have been visited more than once by the gas under study. This makes possible to achieve a rather homogeneous coverage of the powders' surface as a whole. After preparation, the ZnO-covered silicon wafer is immediately inserted into the ultra-high vacuum (UHV) set-up, consisting of the main analysis chamber and a preparation one – both of them affording a residual pressure of less than 10^{-9} mbar. Prior to exposure to water, ZnO powders are thermally activated at 700 K. Fourier Transform Infrared Spectroscopy (FTIR) is performed in the transmission mode on a Bruker Vertex 70 FTIR spectrometer equipped with a MCT detector, spectra were obtained by averaging 100 scans at a resolution of 4 cm^{-1}. Blanks are collected prior to exposure and used as references.

Computational methods

ZnO NPs have been modelled as a combination of most stable surfaces: ($10\bar{1}0$), ($11\bar{2}0$), ($000\bar{1}$), and (0001). These have been represented *via* periodic slabs adding a vacuum region of 10 Å between translationally repeated slabs along the surface direction, following a previously utilized procedure.[38] Test calculations with double vacuum yielded variations in adsorption energies below 0.001 eV, and of at most 2 cm^{-1} in computed vibrational frequencies. Briefly, periodic density functional theory (DFT) calculations have been carried out using the VASP code,[54] while using the projector augmented wave (PAW) method to represent atomic cores.[55] A plane wave basis set of kinetic energy of up to 415 eV was employed with a tetrahedron method algorithm for smearing. Geometry optimizations were performed using a conjugate gradient algorithm, yet final energies obtained were corrected to 0 K (no smearing). Surface structures were considered optimized when forces acting on atoms were below 0.01 eV $Å^{-1}$. Calculations were carried out in a non-spin-polarized fashion using the Perdew–Burke–Ernzerhof (PBE) exchange–correlation functional,[56] known to be appropriate to model wurtzite ZnO bulk and surfaces,[45] as well as interactions of atomic hydrogen, hydroxyl moieties, and water molecules thereon.[48]

Polar $(000\bar{1})$ and (0001) surfaces, as well as nonpolar $(11\bar{2}0)$ surface, are known to display a (1×1) perfect arrangement when fully hydrated.[38,57,58] However, for the nonpolar $(10\bar{1}0)$ surface a (2×1) unit cell is needed, as theoretically and experimentally determined in the past[47,59] and very recently by Kenmoe and co-workers.[60] These surfaces have been represented using eight-layered slabs, whose bottom most layers are kept as in the pre-optimized bulk positions, whereas uppermost four layers, together with H, OH, or H_2O moieties, are fully relaxed. Different arrangements have been explored for H_2O adsorbed on these surfaces, including situations where half or all the H_2O molecules are dissociated, as well as cases where all water remain intact, considering different surface locations of water molecules and H and/or OH groups as well. In all cases, a $17 \times 17 \times 1$ Monkhorst–Pack *k*-points mesh was used, and so, variations in total energy due to the computational setup are below 0.001 eV, as found in tests with stringent conditions. Adsorption energies are already found in the literature,[38] and so here only differences in adsorption energy per H_2O unit are shown. From the found structural energy minima, harmonic frequencies were gained by numerical calculations and diagonalization of the Hessian matrix by independent displacements of 0.03 Å of the adsorbate, and in the case of H adsorbed on a surface O atom, O_s, by taking this into account as well. Shorter displacements lead to variations in frequencies below 4 cm^{-1}, and coupling with substrate is expected to be negligible given that phonon frequencies are in the 100–600 cm^{-1} range.[61] Notice that neglecting anharmonicity may translate into overestimated frequencies, with a difference of $\sim$100 cm^{-1} for frequencies above 3500 cm^{-1}.[38,62] Simulated IR spectra were obtained by estimating the band intensity *via* a change in the vibration dipole moment component normal to surface, and a peak Gaussian convolution of 100 cm^{-1} half-width has been applied.

Conclusions

In summary, by combining infrared spectroscopy and DFT approaches, it is demonstrated that ZnO smoke behaves as multi-facet single crystals. Along with the identification—for the first time—of water structures on ZnO$(11\bar{2}0)$, and of new water structures on ZnO$(10\bar{1}0)$, the present work highlights that highly dispersed ZnO is dominated by a few well-defined low-index orientations and that water adsorption can serve as a discriminant probe to specifically identify oriented facets in those ZnO materials. All the significant infrared bands seen in the experimental spectra of ZnO smoke exposed to water vapour have been directly assigned to calculated modes for water adsorbed on $(10\bar{1}0)$, $(11\bar{2}0)$, (0001), and $(000\bar{1})$ surfaces and, conversely, all the calculated vibrational modes match an experimental counterpart. Cross-agreements between the experimental results and simulations raise confidence in the validity of the assignments. Moreover, the similarity of the infrared spectra collected here to those recorded by Noei *et al.* on another type of ZnO nanopowder[6] suggests that the very simple image emerging from the examination of hydroxylated/hydrated ZnO smokes could be widely applied. The proposed approach differs markedly from common practice. Instead of constraining the synthesis to favour one facet or another, the powder is analysed as it is. This gives a great deal of generality to the present conclusions. In line with the similarity of the infrared spectra collected here with those recorded by Noei *et al.*[6] on a different ZnO powder, this gives a great deal of generality to the present conclusions. The above combined theoretical and experimental approach appears as a robust basis for addressing the surface structure of divided zinc oxide and suggests a wide application for the very simple image emerging from the examination of hydroxylated/hydrated ZnO smokes.

Acknowledgements

We thank Dr Dominique Demaille (INSP, Paris) for recording SEM images shown in Fig. 1 as well as Dr Jacek Goniakowski (INSP, Paris) and Dr Remi Lazzari (INSP, Paris) for fruitful discussions, comments and proofreading. This work has been supported by Spanish Ministry of Economy and Competitiveness (MINECO) and Fondo Europeo de Desarrollo Regional (FEDER) CTQ2015-64618-R grant and partly by Generalitat de Catalunya grants 2014SGR97, and XRQTC. The research in this work is in the framework of the NOMAD Center of Excellence project which received funding from the European Union's Horizon 2020 research and innovation programme under grant agreement No. 676580. F. V. thanks MINECO for a postdoctoral Ramón y Cajal (RyC) research contract (RYC-2012-10129). F. I. acknowledges additional support from the 2015 ICREA Academia Award for Excellence in University Research.

References

1 C. Burda, X. Chen, R. Narayanan and M. A. El-Sayed, *Chem. Rev.*, 2005, **105**, 1025.
2 G. A. Somorjai and R. M. Rioux, *Catal. Today*, 2005, **100**, 201.
3 A. Zecchina, E. Groppo and S. Bordiga, *Chem. – Eur. J.*, 2007, **13**, 2440.
4 K. Zhou and Y. Li, *Angew. Chem., Int. Ed.*, 2012, **51**, 602.
5 G. Spoto, E. N. Gribov, G. Ricchiardi, A. Damin, D. Scarano, S. Bordiga, C. Lamberti and A. Zecchina, *Prog. Surf. Sci.*, 2004, **76**, 71.
6 H. Noei, H. Qiu, Y. Wang, E. Löffler, C. Wöll and M. Muhler, *Phys. Chem. Chem. Phys.*, 2008, **10**, 7092.
7 P. Borghetti, E. Meriggio, G. Rousse, G. Cabailh, R. Lazzari and J. Jupille, *J. Phys. Chem. Lett.*, 2016, **7**, 3223.
8 S. Coluccia, A. J. Tench and R. L. Segall, *J. Chem. Soc., Faraday Trans. 1*, 1979, **75**, 1769.
9 E. Garrone, A. Zecchina and F. S. Stone, *Philos. Mag. B*, 1980, **42**, 683.
10 E. Knözinger, K.-H. Jacob, S. Singh and P. Hofmann, *Surf. Sci.*, 1993, **290**, 388.
11 R. Hacquart, J.-M. Krafft, G. Costentin and J. Jupille, *Surf. Sci.*, 2005, **595**, 172.

12 S. Stankic, J. Bernardi, O. Diwald and E. Knözinger, *J. Phys. Chem. B*, 2006, **110**, 13866.
13 A. F. Moodie and C. E. Warble, *J. Cryst. Growth*, 1971, **10**, 26.
14 R. Hacquart and J. Jupille, *Chem. Phys. Lett.*, 2007, **439**, 91.
15 P. Geysermans, F. Finocchi, J. Goniakowski, R. Hacquart and J. Jupille, *Phys. Chem. Chem. Phys.*, 2009, **11**, 2228.
16 G. Cabailh, R. Lazzari, J. Jupille, L. Savio, M. Smerieri, A. Orzelli, L. Vattuone and M. Rocca, *J. Phys. Chem. A*, 2011, **115**, 7161.
17 E. Knözinger, K.-H. Jacob and P. Hofmann, *J. Chem. Soc., Faraday Trans.*, 1993, **89**, 1101.
18 O. Diwald and E. Knözinger, *J. Phys. Chem. B*, 2002, **106**, 3495.
19 N. Siedl, D. Koller, A. K. Sternig, D. Thomele and O. Diwald, *Phys. Chem. Chem. Phys.*, 2014, **16**, 8339.
20 V. H. Grassian, *J. Phys. Chem. C*, 2008, **112**, 18303.
21 K. P. McKenna and A. L. Shluger, *Nat. Mater.*, 2008, **7**, 859.
22 D. C. Hurum, A. G. Agrios, K. A. Gray, T. Rajh and M. C. Thurnauer, *J. Phys. Chem. B*, 2003, **107**, 4545.
23 J. Pan, G. Liu, G. Q. Lu and H.-M. Cheng, *Angew. Chem., Int. Ed.*, 2011, **50**, 2133.
24 H. G. Yang, C. H. Sun, S. Z. Qiao, J. Zou, G. Liu, S. C. Smith, H. M. Cheng and G. Q. Lu, *Nature*, 2008, **453**, 638.
25 C. Deiana, M. Minella, G. Tabacchi, V. Maurino, E. Fois and G. Martra, *Phys. Chem. Chem. Phys.*, 2013, **15**, 307.
26 P. S. Shewale and Y. S. Yu, *J. Alloys Compd.*, 2016, **684**, 428.
27 D. Chakraborty, R. Gayen, S. Hussain, R. Bhar, A. K. Ghoshal and A. K. Pal, *J. Phys.: Conf. Ser.*, 2012, **390**, 012065.
28 R. Knut, R. Lindblad, S. Grachev, J.-Y. Faou, M. Gorgoi, H. Rensmo, E. Søndergard and O. Karis, *J. Appl. Phys.*, 2014, **115**, 043714.
29 K. Kalyanasundaram, *J. Phys. Chem. C*, 2014, **118**, 16303.
30 C. T. Campbell, K. A. Daube and J. M. White, *Surf. Sci.*, 1987, **182**, 458.
31 K. Maeda and K. Domen, *Chem. Mater.*, 2010, **22**, 612.
32 Ü. Özgür, Y. I. Alivov, C. Liu, A. Teke, M. A. Reshchikov, S. Dogan, V. Avrutin, S.-J. Cho and H. Morkoç, *J. Appl. Phys.*, 2005, **98**, 041301.
33 Z. L. Wang, *Mater. Today*, 2004, **7**, 26.
34 A. B. Djurisic and Y. H. Leung, *Small*, 2006, **2**, 944.
35 P. X. Gao and Z. L. Wang, *J. Appl. Phys.*, 2005, **97**, 044304.
36 G. R. Li, T. Hu, G. L. Pan, T. Y. Yan, X. P. Gao and H. Y. Zhu, *J. Phys. Chem. C*, 2008, **112**, 11859.
37 D. Scarano, G. Spoto, S. Bordiga, A. Zecchina and C. Lamberti, *Surf. Sci.*, 1992, **276**, 281.
38 F. Viñes, A. Iglesias-Juez, F. Illas and M. Fernandez-García, *J. Phys. Chem. C*, 2014, **118**, 1492.
39 S. Kittaka, T. Sasaki and N. Fukuhara, *Langmuir*, 1992, **8**, 2598.
40 A. Iglesias-Juez, F. Viñes, O. Lamiel-García, M. Fernández-García and F. Illas, *J. Mater. Chem. A*, 2015, **3**, 8782.
41 G. Wulff, *Z. Kristallogr. Mineral.*, 1901, **34**, 449.
42 F. Viñes, J. R. B. Gomes and F. Illas, *Chem. Soc. Rev.*, 2014, **43**, 4922.
43 H. F Wilson, C. Tang and A. S. Bernard, *J. Phys. Chem. C*, 2016, **120**, 9498.
44 T. Sato, T. Tanigaki, H. Suzuki, Y. Saito, O. Kido, Y. Kimura, C. Kaito, A. Takeda and S. Kaneko, *J. Cryst. Growth*, 2003, **255**, 313.
45 B. Meyer and D. Marx, *Phys. Rev. B: Condens. Matter Mater. Phys.*, 2003, **67**, 035403.
46 Y. Wang, M. Muhler and C. Wöll, *Phys. Chem. Chem. Phys.*, 2006, **8**, 1521.
47 O. Dulub, B. Meyer and U. Diebold, *Phys. Rev. Lett.*, 2005, **95**, 136101.
48 B. Meyer, H. Rabaa and D. Marx, *Phys. Chem. Chem. Phys.*, 2006, **8**, 1513.
49 D. J. Cooke, A. Marmier and S. C. Parker, *J. Phys. Chem. B*, 2006, **110**, 7985.
50 D. Raymand, A. C. T. van Duin, D. Spångberg, W. A. Goddard III and K. Hermansson, *Surf. Sci.*, 2010, **604**, 741.
51 S. G. Holthaus, S. Köppen, T. Frauenheim and L. C. Ciacchi, *J. Chem. Theory Comput.*, 2012, **8**, 4517.
52 S. Stankic, M. Cottura, D. Demaille, C. Noguera and J. Jupille, *J. Cryst. Growth*, 2011, **329**, 52.
53 F. Finocchi, R. Hacquart, C. Naud and J. Jupille, *J. Phys. Chem. C*, 2008, **112**, 13226.
54 G. Kresse and J. Furthmüller, *Phys. Rev. B: Condens. Matter Mater. Phys.*, 1996, **54**, 11169.
55 P. E. Blöchl, *Phys. Rev. B: Condens. Matter Mater. Phys.*, 1994, **50**, 17953.
56 J. P. Perdew, K. Burke and M. Ernzerhof, *Phys. Rev. Lett.*, 1996, **77**, 3865.
57 M. Kunat, S. Gil-Girol, T. Becker, U. Burghaus and C. Wöll, *Phys. Rev. B: Condens. Matter Mater. Phys.*, 2002, **66**, 081402.
58 T. Becker, S. Hövel, M. Kunat, C. Boas, U. Burghaus and C. Wöll, *Surf. Sci.*, 2001, **486**, L502.
59 B. Meyer, D. Marx, O. Dulub, U. Diebold, M. Kunat, D. Langenberg and C. Wöll, *Angew. Chem., Int. Ed.*, 2004, **43**, 6642.
60 S. Kenmoe and P. U. Biedermann, *Phys. Chem. Chem. Phys.*, 2017, **19**, 1466.
61 B. H. Bairamov, A. Heinrich, G. Irmer, V. V. Toporov and E. Ziegler, *Phys. Status Solidi B*, 1983, **119**, 227.
62 S. Manzhos, T. Carrington Jr. and K. Yamashita, *Surf. Sci.*, 2011, **605**, 616.